A novel design of stator Ferrite PM single phase doubly salient small motor: FEM characterization and controlled dynamics

A. S. Işfănuți*, MS student, L. N. Tutelea*, IEEE Member, F. J. H Kalluf**, I. Boldea*, IEEE Life Fellow
* Dept. of Electrical Machines and Drives, University Politehnica of Timisoara
**Dept. of Research and Development, Embraco, Brasil
aisfanuti@yahoo.com, luci@lselinux.upt.ro, Flavio_J_H_Kalluf@embraco.com.br, ion.boldea@upt.ro

***Abstract*-The present paper introduces a novel two coil 1 phase stator Ferrite PM motor [1]. The main targets are reduced material and fabrication costs in a robust topology at 90% efficiency for a 35W, 1600 rpm case study. Due to complicated flux lines (with tapered airgap for self-starting) and magnetic saturation, direct FEM characterization (preliminary design) was applied. Matlab Simulink modeling for controlled dynamics which made use FEM imposed cogging torque, emf and inductance with rotor position waveforms proved smooth motor starting to rated speed for speed performance, full load in both open loop (V/f) and close loop control.**

I. INTRODUCTION

Small power, even highs .efficiency at moderate cost motor appliances are vastly needed for home appliances and info-gadgets.

The line start split phase induction [2] and lately PM synchronous motors [3] have been used for decades for the scope. But the advantage for variable speed on the energy conversion in small compressor or pump loads has led to the recent strong penetration of inverter fed ac motor drives at small power [4].

PMSMs are the prime candidates due to their higher efficiency and compact size. But the recent sharp increase in high energy (NdFeB) magnets has led to the search for lower cost small electric motors. Ferrite-PMSM in varies 3-phase configuration with high flux concentration motors are required to match the NdFeB PMSM for same efficiency, at larger weight, but at lower initial cost [5].

On the other hand 1 phase and 3 phase SRM drives have been used for the scope. However, the lower efficiency, complicated control, higher noise limits the utilization of SRM in small power applications, with the exception, perhaps, of super high speeds (vacuum cleaner).

A stator PM doubly salient motor configuration is introduced in the paper. It stems from the flux reversal (or flux switching) principles [6], but the use of only two coils and of flat PMs to be introduced in the stator core simply from outside after winding the motor simplifies notably the fabrication, while the salient rotor is robust.

The tapered airgap in the rotor allows for safe self-starting from a unique self-parking position.

The paper is organized as follows:

- section II presents the motor geometry along with the design requirements.
- section III shows the FEM analysis and design methodology
- section VI displays FEM analysis regarding load and no load operation in order to determine motor's parameters and performance
- section V presents comparative design results between the proposed 1 phase motor and an existing solution (3 phase surface Ferrite PM BLAC)
- section VI presents the control dynamics on the studied 1 phase motor, under two cases, in order to prove its performance
- section VII contains discussion and conclusions.

II. MOTOR GEOMETRY

The proposed motor topology [1] comes as an alternative solution for an existing 3phase, 6/4 Ferrite surface PM BLAC motor. The parameters for the witness BLAC motor were used as either requirements (motor size, efficiency, speed, power, torque), either as input data (as permanent magnet material characteristics) and are presented in the table below.

TABLE I
WITNESS 6/4BLAC MOTOR PARAMETERS

Parameter	Value	Description
P_N	35 W	rated power
V_{DC}	290 VDC	DC voltage
n_N	1600 rpm.	rated speed
N_n	0.2 Nm	rated torque
η_{max}	0.93-0.94	electric efficiency
turns/phase	540	number of turns per phase
k_{fill}	0.5	slot filling factor
D_{OS}	116 mm	stator outer diameter
h_{PM}	7.3 mm	PM height
h_{CS}	15.5 mm	stator coil height
A_{slot}	376 mm^2	stator slot area
W_{total}	2.16 kg	motor mass
γ_{mag}	4800 kg/m3	core density
B_r	0.415 T	PM remanence
H_c	260 kA/m	PM coercitivity

Fig 1. presents the proposed geometry for 1 phase motor. It consists of a two pole stator having the corresponding two

coils in series, fed with a trapezoidal alternating current, assisted by 4 magnet pieces and an anisotropic four pole pair rotor.

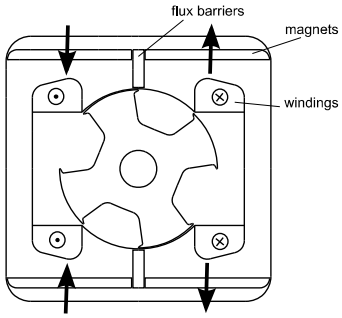

Fig. 1. 1 phase motor geometry.

The flux paths during operation can be observed in Fig. 2, where the two rotor positions correspond to the positive and negative maximum magnetic flux in stator coil which is also the current commutation point.

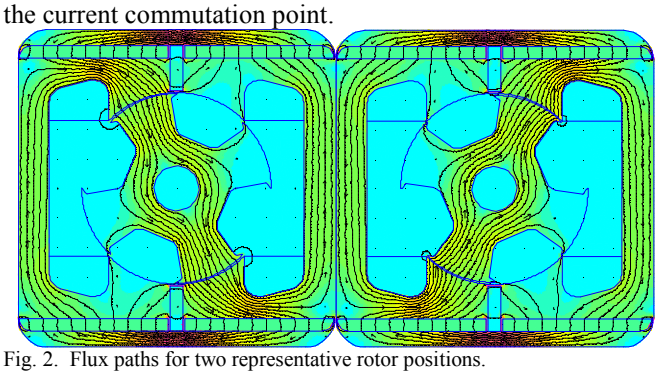

Fig. 2. Flux paths for two representative rotor positions.

III. FEM ASSISTED DESIGN METHODOLOGY

The design methodology consisted of choosing proper values for the main dimensions by running a 2D FEM inquiry with the aim of:

- optimize (maximize the EMF)
- minimize the magnetic cogging torque around 45º, 135º, by shaping the flux barrier in the stator poles (Fig. 1)
- maximize the torque, by changing the airgap ratio *hag/hag1*.

Also the rotor pole teeth shape was optimized in order to reduce the fringing flux.

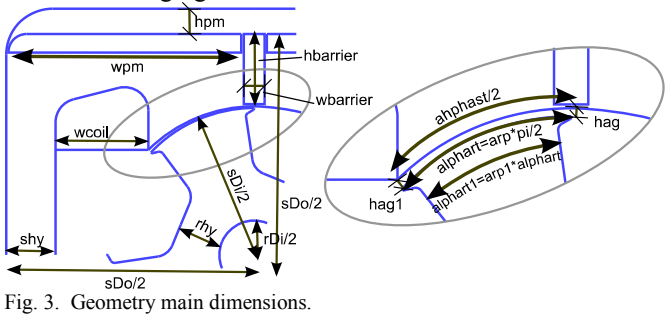

Fig. 3. Geometry main dimensions.

The final values for the main geometry dimensions (Fig. 3) are summarized in the Table II.

TABLE II
MAIN DIMENSIONS

Parameter	Unit	Value
sDo	mm	107
sDi	mm	64.54
rDi	mm	14.94
hag	mm	0.35
hag1	mms	1.5*hag
N	turns	650
swp	mm	45.6408
lstack	mm	30
wpm	mm	4.5
hpm	mm	4
wbarrier	mm	4.5
hbarrier	mm	15.22
shy	mm	15.6
rhy	mm	9.66
wcoil	mm	20
alphast	deg	90
alphart	deg	45
alphart1	deg	0.7* alphart

IV. FEM ANALYSIS

A. No load

First the airgap magnetic flux density is presented in Fig. 4 for the two rotor positions shown in Fig. 2. It can be observed that the induction reaches almost 0.6T in the smaller airgap region.

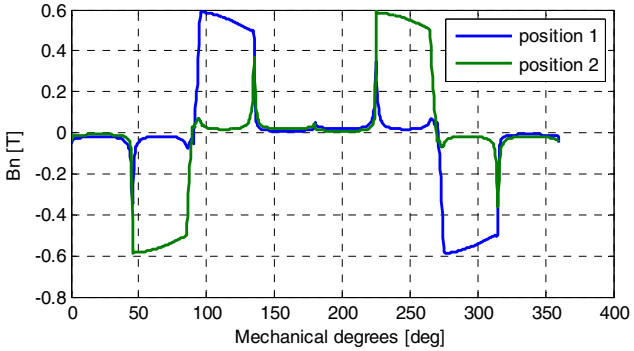

Fig. 4. Airgap flux density versus rotor position.

Fig. 5 shows the cogging torque variation with rotor position

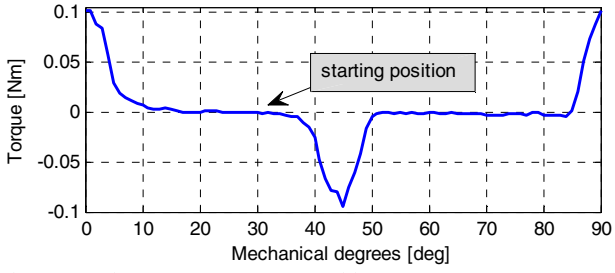

Fig. 5. Cogging torque versus rotor position.

. It can be seen that a negative peak is still present at 45º (second rotor position from Fig. 2). A zero cogging torque

stable position, which can be used for starting up is the 27º rotor position.

No load magnetic flux linkage and EMF are presented in Fig. 6. The EMF was computed using the formula:

$$EMF = \frac{d\Psi}{dt} = \frac{d\Psi}{d\theta} \cdot \frac{d\theta}{dt} = \frac{d\Psi}{d\theta} \cdot \frac{360 \cdot n_N}{60 \cdot step} \quad (1)$$

where step is the mechanical step used in analysis (step=1 mechanical degree). The EMF peak reaches 100 V.

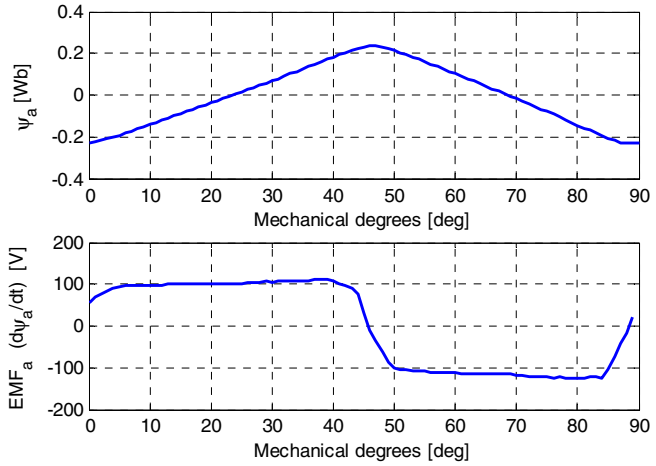

Fig. 6. PM phase flux and emf versus rotor position.

B. Load

The load analysis was performed by feeding the winding with a trapezoidal current (Fig. 7). The zero position of the current is synchronized with the maximum flux linkage position. The falling shape of current was chosen as an opposite variation to the EMF rising slope, to reduce the electromegnetic power comutation caused oscillations.

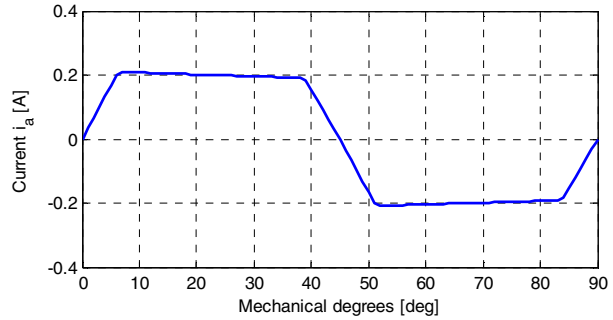

Fig. 7. Tentative current waveform.

Next, the torque components are presented (Fig. 8). The total torque (blue line) has a relatively large negative peak around 45º, due to the presence of cogging torque combined with the current commutation. In the respective region, a positive value for the cogging torque would have been preferable, to compensate the absence of the electromagnetic torque, as it does at 0º position. The maximum value is 0.34 Nm, while the average value is 0.22 Nm.

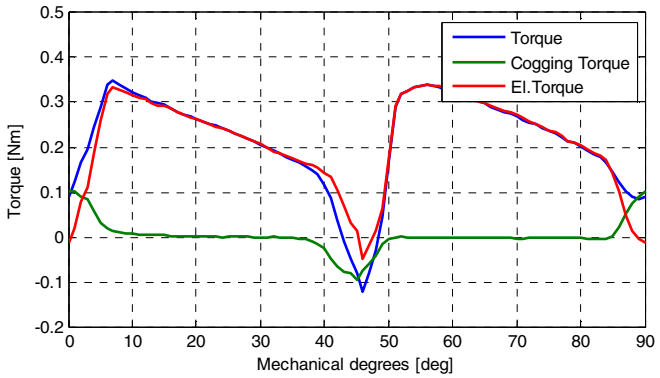

Fig. 8. Torque components versus rotor position.

The load versus no load flux linkage is shown in Fig. 9 a). The load flux linkage has the maximum value around 38º, and intersects the no load linkage flux at 45º, as it should do. Their difference divided to current can be seen as winding inductance (Fig. 9 b).

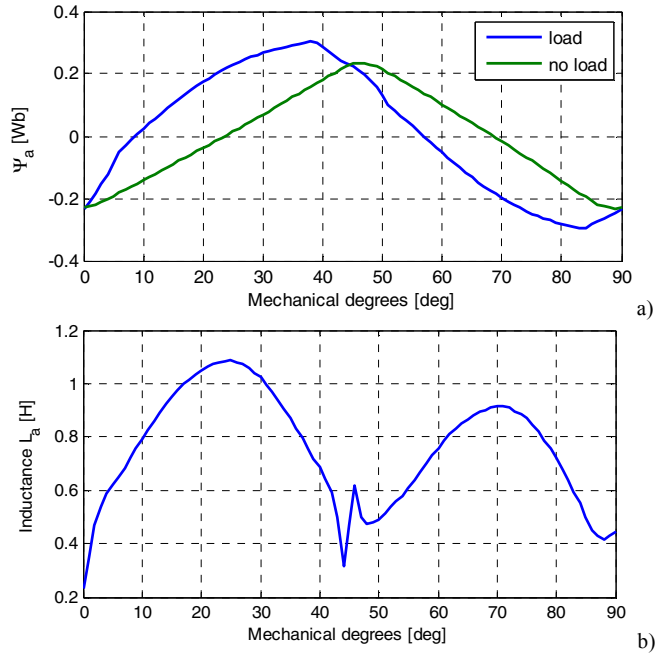

Fig. 9. Flux linkage versus position a), phase inductance versus position b).

Last, the variation with time of the load flux linkage, in comparison with the no load EMF is given in Fig. 10.

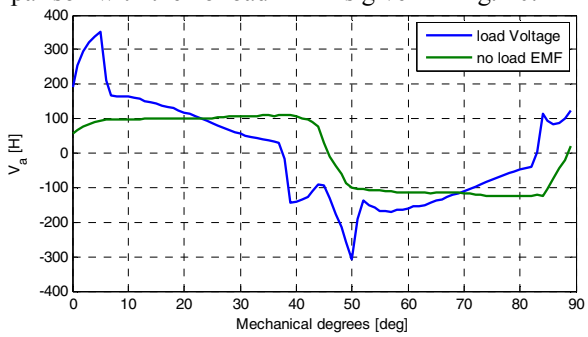

Fig. 10. Emf and the required phase voltage.

Around 0º and 45º large values of the voltage are present which suggest that there will be problems commutating the current

C. *Iron loss computation*

Only the iron loss due to flux density variation in the stator core was considered (a similar study is feasible for rotor). In order to determine the flux density variation, the stator core was divided upon a region of interest (equal to a quarter of stator core) into few sub-regions (Fig. 11).

For each region an average value of flux density was calculated as:

$$B_k = \frac{1}{V_k}\int_{V_k} B dV, \quad k = 1,...32 \tag{2}$$

with V_k being the volume of the k sub-region. B_k varies with time (or with rotor position) so the maximum value was retained considering the rated load analysis. The iron losses were finally computed using a simplified relation, based on a single coefficient:

$$\begin{aligned} p_{iron} &= 2N_{sc}\sum_k p_{ironk} \\ &= 2N_{sc}\sum_k p_{iron1T400Hz}\cdot\left(B_{\max k}\frac{f_n}{400}\right)^2 V_k\cdot\rho_{iron} \end{aligned} \tag{3}$$

where N_{sc} - number of stator poles, f_n - rated frequency (54 Hz), ρ_{iron} - stator core iron density and $p_{iron}1T400Hz$ represents the specific losses of the stator core iron (W/kg).

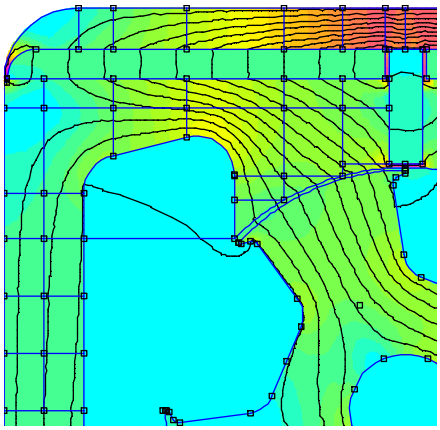

Fig. 11. Stator regions used for iron loss computation.

For simplicity, the rotor iron losses were computed using the stator iron losses and the assumption of a proportional variation with core volume. So finally:

$$p_{iron} = p_{iron\_stator}\left(1+\frac{V_{rotor}}{V_{stator}}\right) \tag{4}$$

D. *Copper losses computation*

Copper losses were computed using the well-known formula:

$$p_{co} = R\cdot I^2 \tag{5}$$

with the resistance obtained from:

$$R = \frac{\rho\cdot 2\cdot l_{turn}\cdot N}{\frac{I}{j_{co}}} \tag{6}$$

where the current density j_{co}=1.5 A/mm^2.

V. Comparative Design Results

A comparison in terms of material weight and losses between the single phase motor and 6/4 3 phase BLAC PM motor is presented below.

- The following material prices were considered:
- copper price: 10 USD/kg
- lamination price: 1.7 USD/kg
- rotor shaft iron price: 1.7 USD/kg
- passive materials (insulation and frame) price: 1.7 USD/kg (the cost considers the motor mass *wt_Tot*).
- Ferrite PM price: 6 USD/kg

TABLE III
Comparison between BLAC and 1 phase motor

	1phase motor	**6/4 BLAC**
StatorOD [mm]	107	116
RotorOD [mm]	63 to 63.84	61.6
Gap [mm]	0.35 to 0.77	0.7
Lrotor [mm]	30	30.5
SYoke [mm]	15.6	11
RYoke [mm]	9.6634	15.5
Weights		
wt_Cu [kg]	0.2731	0.5084
wt_Fe [kg]	1.6387	1.4967
wt_FeS [kg]	1.1645	1.1455
wt_FeR [kg]	0.4742	0.3512
wt_Mag [kg]	0.1402	0.1621
wt_Tot [kg]	2.0453	2.1672
Losses		
WCu [W]	1.514135	1.0778
WFe [W]	2.194121	1.0491
WTotal [W]	3.70825	2.127
MechLosses [W]	0.399	1.491
Eff_el [%]	0.9064	94.012
Costs		
copper cost	2.7315	5.084
lamination cost	1.9797	1.94735
rotor iron cost	0.79462	0.59704
PM cost	0.8413	0.1621
passive material cost	3.4771	3.6842
active material cost	6.3472	7.79099
total cost	9.8244	11.47159

As it can be observed, the 1 phase PM motor has the total price lower with approximately 1.65USD. However, this pays the 4% lower electric efficiency. On the other hand the fabrication cost reduction on account of only two preformed coils, the rotor robustness, the easy mounting of Ferrite PMs on stator and simplified control of single phase inverter, should constitute solid reasons to consider the 1 phase proposed motor drive in low power drive applications.

VI. Controlled Dynamics

A. *Dynamic model*

In order to verify the motor capability of producing the required torque and power, the dynamic operation must be studied.

The differential equations that describe the dynamic behavior of 1 phase PM motor are presented as follows. The voltage equation is:

$$v(t) = R \cdot i(t) + L(\theta)\frac{di(t)}{dt} + e(t) \tag{7}$$

where the inductance variation with current is neglected. The emf *e(t)* is proportional with speed:

$$e(t) = k(\theta) \cdot \omega(t) \tag{8}$$

and

$$\theta(t) = \int \omega(t)\, dt \tag{9}$$

The mechanical equation is:

$$J\frac{d\omega(t)}{dt} = T_e - T_{cogg}(\theta) - T_L - B \cdot \omega(t) \tag{10}$$

where the electromagnetic torque can be written as:

$$T = k(\theta) \cdot i(t) \tag{11}$$

The digram block for the above equations can be observed in the figure below:

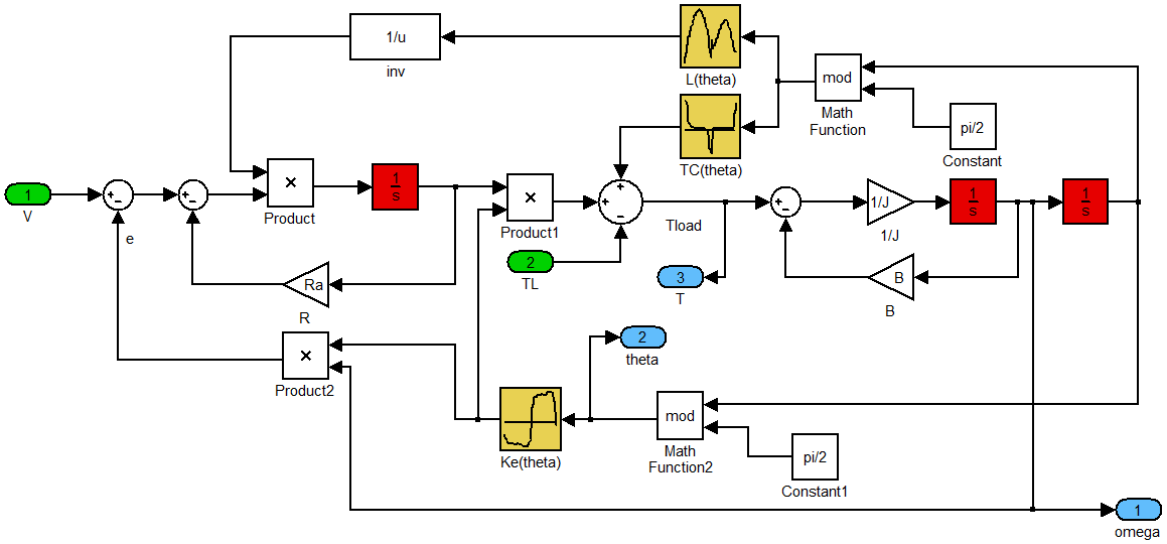

Fig. 12. Dynamic model of 1 phase stator Ferrite PM motor with its inductance, emf and cogging torque waveforms imported from FEM analysis,as in [7].

B. Operation with impressed voltage versus rotor position (under torque proportional with speed)

For the first case, the model was fed with a ramp voltage (0 to 290 V in 0-0.3 ms) followed by a constant DC voltage. The voltage polarity was switched according to the rotor position (positive polarity for 45 mechanical degrees followed by a negative polarity for the next 45 mechanical degrees). The load was considered proportional with the speed through the fictitious coefficient *B*. The results are presented below:

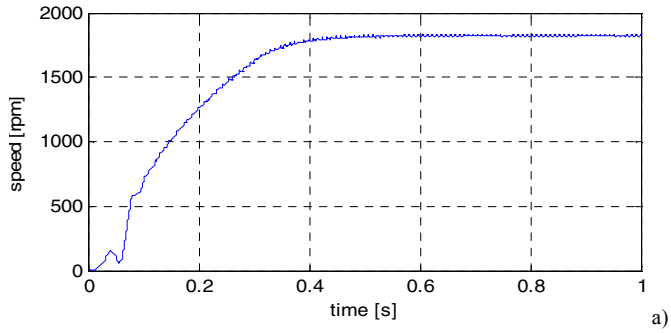

a)

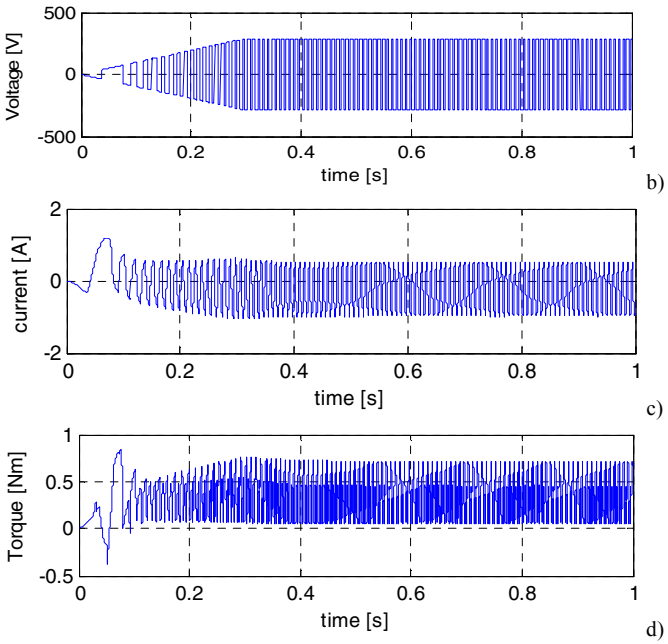

b) c) d)

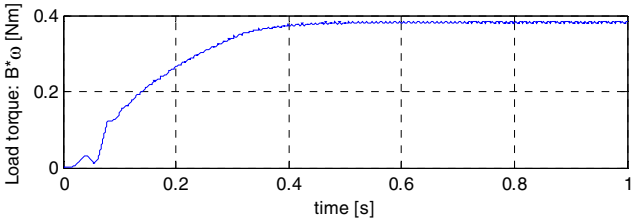

e)

Fig. 13. Open loop acceleration transients under load with prescribed voltage/frequency [8] speed variation with time a) motor fed voltage b) current variation with time c) electromagnetic torque d) and load torque (proportional with speed) e).

This is an open loop acceleration transient with load proportional to speed which shows that the motor is capable to produce the rated average (0.2 Nm) torque at rated speed (1600 rpm), with an acceleration time of around 0.4 seconds.

C. *Operation with speed and current control*

The second case uses a speed controller (a classic PI controller) and a hysteresis current controller. The coefficients for the PI controller are k_p=10, k_i=100, and the output is limited to 0.4 A. The current controller has a hysteresis band of 0.02 A (Fig. 14).

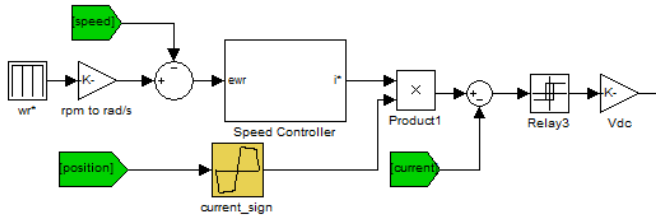

Fig. 14. Speed and current control loops

The profile for reference speed is the following: acceleration at 1500rpm in 0.05s, followed by constant 1500 rpm. The results are displayed in Fig. 15

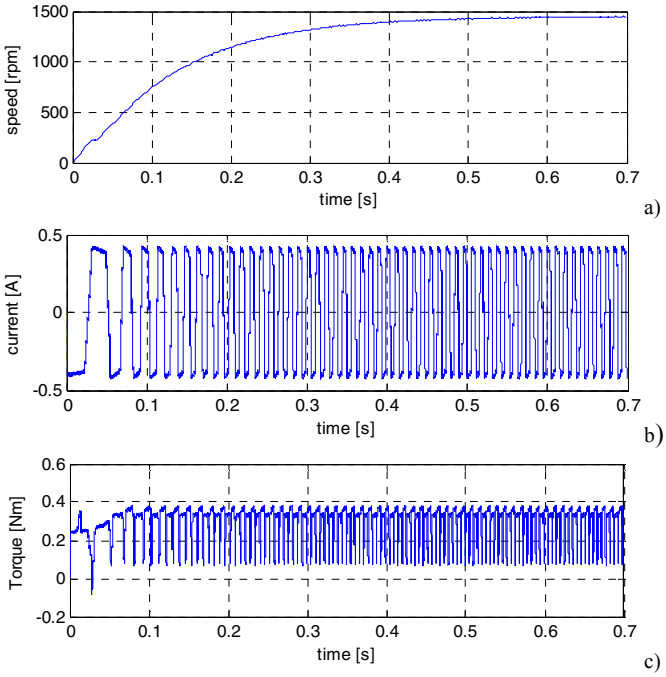

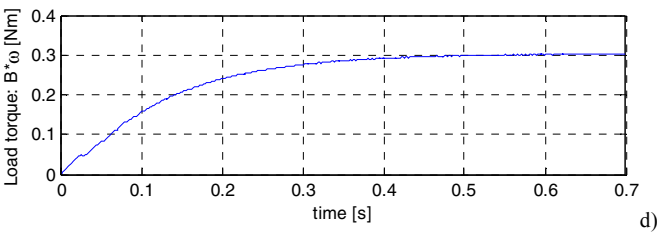

d)

Fig. 15. Close loop controlled acceleration to 1500 rpm under load with limited current (0.5 A): speed versus time a), current variation with time b) electromagnetic torque c) and load torque (proportional with speed) d).

The reference speed was still considered a ramp (of 0.05s only), but the current limitation at 0.5A imposed a slower acceleration (about 0.4-0.5s) to 1500 rpm.

Still, the drive proved capable to produce the rated torque at rated speed for the given 290 DC supply. Although this second case would increase the total cost, compared to the open loop control, it ensures a more precise speed control, while still costitutiting a easyer control method than the one for the 3 phase BLAC.

VII. Discussion and Conclusions

The paper introduced a novel, 1 phase stator Ferrite PM small motor & drive in order to reduce fabrication and initial motor cost and simplify the inverter control

The novel motor has only two stator coils where the PM flux switches polarity in a doubly salient topology with 4 rotor salient poles (4 equivalent pole pairs)

FEM is used to characterize the new motor, due to complicated flux lines trajectories and magnetic saturation.

The parking position (obtained through airgap tapering) at 27º, allows for sufficient time to start the motor on speed proportional full load torque (0.2 Nm), even in open loop (V/f) control within 0.4 seconds to 1600 rpm.

Controlled dynamics is investigated through Matlab Simulink with inductance, cogging-torque and emf waveform imported from FEM.

Close loop speed and current control acceleration transients with limited peak current (0.5 A), under speed proportional full load prove smooth response up to rated speed and torque.

In this preliminary investigation we managed to produce a 20% less expensive initial cost motor solution (than the one with 3 phase BLAC PM Ferrite motor drive at 35 W), at 90% efficiency at 1600 rpm (instead of 94%). The motor, inverter, control and lower fabrication costs should compensate for the loss of efficiency.

References

[1] F. Kalluf, I. Boldea, “Motor elétrico de relutância chaveado”, Brasilian Patent Ref: BR102013018363.6//July 18, 2013

[2] B. M. Gordon, R. A. McMahon, “Comparison of two low cost small induction motor drive configuration”, Record of EPE - 1997, Trondheim, Vol3, pp 724-729

[3] F. Meyer, “Permanent manget synchronous machines with non-overlapping concentrated windings for low speed direct-drive applications, Ph.D. dissertation, Royal Institute of Technology, Stochholm, 2008

[4] I. Boldea, S. Nasar, " Electric Drives (2nd Edition)", Boca Raton, FL.:Taylor&Francis (CRC Press), 2005

[5] I. Petrov, J. Pyrhönen, "Performance of low cost permanent magnet material in PM synchronous machines", IEEE Transactions on Industrial Electronics, vol 60, No.6, 2013, pp. 2131-2138.

[6] R. P. Deodhar, S. andersson, I. Boldea, T. J. E. Miller, "The flux-reversal machine, a new brushless doubly-salient permanent-magnet machine", Trans. on Industry Applications, vol. 33, no. 4, July/August 1997, pp. 925-934.

[7] L, I. Iepure. "Sensorless control of single phase PM brushless dc motor drives" Ph.D. dissertation,Politehnica University of Timisoara, Timisoara, 2010

[8] L. I. Iepure, I. Boldea, F. Blaabjerg, "Hybrid I-f starting and observer based sensorless control of single-phase BLDC-PM motor drives", Trans on Industry Applications, vol 59, no. 9, September 2012, pp. 3436-3444